ISSN 2072-5981
doi: 10.26907/mrsej

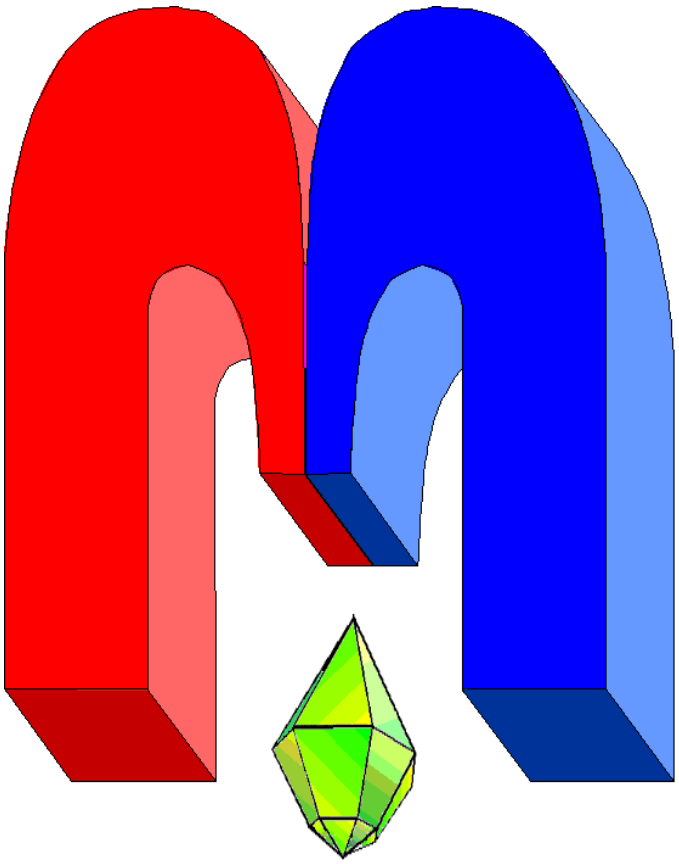

Magnetic Resonance in Solids

Electronic Journal

Volume 27
Issue 2
Article No ***25203***
1-13 pages
2025
doi: **10.26907/mrsej-25203**

http://mrsej.kpfu.ru
http://mrsej.elpub.ru

Established and published by Kazan University*
Endorsed by International Society of Magnetic Resonance (ISMAR)
Registered by Russian Federation Committee on Press (#015140), August 2, 1996
First Issue appeared on July 25, 1997

"***Magnetic Resonance in Solids. Electronic Journal***" (**MRS*ej***) is a peer-reviewed, all electronic journal, publishing articles which meet the highest standards of scientific quality in the field of basic research of a magnetic resonance in solids and related phenomena.

Indexed and abstracted by
Web of Science (*ESCI*, Clarivate Analytics, from 2015), *Scopus* (Elsevier, from 2012), *RusIndexSC* (*eLibrary*, from 2006), *Google Scholar*, *DOAJ*, *ROAD*, *CyberLeninka* (from 2006), *SCImago Journal & Country Rank*, etc.

* Address: "Magnetic Resonance in Solids. Electronic Journal", Kazan Federal University; Kremlevskaya str., 18; Kazan 420008, Russia

† In Kazan University the Electron Paramagnetic Resonance (EPR) was discovered by Zavoisky E.K. in 1944.

Magnetoelectric and spin-lattice effects in $Fe/BaTiO_3$ heterostructure: non-collinear DFT calculations

I.I. Piyanzina[1,2,*], R. Burganova[3], A.A. Kamashev[2], R.F. Mamin[2]

[1]Yerevan State University, Yerevan 0025, Armenia

[2]Zavoisky Physical-Technical Institute, Kazan 420029, Russia

[3]Kazan Federal University, Kazan 420008, Russia

**E-mail: irina.gumarova@ysu.am*

(received April 17, 2025; revised April 17, 2025; accepted May 30, 2025; published June 3, 2025)

This article uses density functional theory calculations to explore the structural, electronic, and magnetic features of a ferromagnet/ferroelectric $Fe/BaTiO_3$ heterostructure, which possesses a complex non-collinear magnetic structure. The presented research focuses on the evolution of spin systems under the influence of external fields, namely the reorientation of magnetic moments driven by electric-field-induced polarization switching and lattice strain. We demonstrated that the electronic and magnetic properties of the thin ferromagnetic Fe film can be effectively tuned by applying an external electric field – simply by altering the polarization direction of the ferroelectric $BaTiO_3$. By incorporating spin-orbit coupling into the computation scheme, we evaluated the relative structural distortions, magnetic moments in atomic layers, atom- and orbital-resolved density of states, magnetic anisotropy energies, and easy magnetization directions.

PACS: 73.20.-r, 73.20.At

Keywords: ferroelectric, heterostructure, noncollinear magnetism, density functional theory, ME coupling, reverse magnetostriction.

1. Introduction

Converse magnetoelectric coupling refers to the phenomenon where an applied electric field or electric polarization induces changes in the magnetization of a material, as opposed to the direct effect where a magnetic field induces electric polarization. This effect is central to multiferroic and composite materials that combine ferromagnetic and ferroelectric properties. The converse magnetoelectric effect influences spin dynamics by enabling electric-field control over spin precession, domain wall motion, and spin wave excitations. This effect is the topic of many studies today [1–7] due to its potential applications in modern electronics. This phenomenon enables the manipulation of a material's magnetic properties by an external electric field and the control of the electrical properties by a magnetic field, providing numerous opportunities to solve problems of modern electronics [8–10].

Materials exhibiting magnetoelectric coupling are promising candidates for components in magnetoresistive memory devices and spin valves [11–14]. The ability to control magnetic properties through electric fields can lead to more energy-efficient and scalable memory technologies. Recent studies have shown that heterostructures, where a magnetic material is epitaxially grown on a ferroelectric substrate, can exhibit multiferroic properties. For example, *ab initio* studies of $Fe/BaTiO_3$, $Co/BaTiO_3$, and $Ni/BaTiO_3$ superlattices have revealed the possibility of controlling the magnetic properties of a ferromagnet by changing the direction of ferroelectric polarization [15–17]. Moreover, first-principles calculations predict strong coupling in double transition metal dichalcogenide $NbVS_4$, where an applied electric field can induce a transition between ferromagnetic and antiferromagnetic states, offering a promising platform for tunable spintronic devices [18].

Another approach to modulating the magnetic properties of thin ferromagnetic films in ferromagnet/ferroelectric (FM/FE) heterostructures is reverse magnetostriction. This effect, also known as the Villari effect, refers to the phenomenon where mechanical stress applied to a magnetic material alters its magnetization. In other words, stretching or compressing a ferromagnetic sample changes the orientation and magnitude of its magnetic domains, thus modifying its overall magnetization. Studies indicate that mechanical deformation of the ferroelectric layer generates an electric field, which can modulate the magnetization of the neighboring ferromagnetic film [19–23]. This opens new possibilities of manipulating spin textures such as domain walls and skyrmions, making reverse magnetostriction a tool for controlling magnetoelectric devices.

Recent advancements have expanded the understanding of magnetoelectric coupling mechanisms. For example, research on hybrid-improper ferroelectric $Ca_3Mn_{1.9}Ti_{0.1}O_7$ has shown that nonpolar structural distortions can give rise to spontaneous electric polarization and magnetization, leading to a pronounced magnetoelectric response [24]. Optical second harmonic generation in $BiFeO_3$ films has demonstrated robust coupling even in freestanding structures, stable against thermal fluctuations [25]. Light-induced magnetoelectric effects in $Ni/BaTiO_3$ heterostructures have shown that domain wall motion in the ferroelectric layer can transfer strain to the ferromagnetic film, enabling remote control of magnetic properties through optical excitation [26]. Additionally, studies on multiferroic $GdFeO_3$ have revealed a magnetoelectric caloric effect, where changes in an external electric field induce temperature variations, presenting opportunities for energy-efficient solid-state cooling technologies [27].

Building on these developments in the field of spintronic and magnetoelectric materials, this work focuses on the $Fe/BaTiO_3$ thin film heterostructure by using density functional theory (DFT) calculations. Fe in the body-centered cubic (bcc) phase is a well-studied ferromagnetic material with known values of the lattice parameter and magnetic moment in the bulk phase. $BaTiO_3$ (BTO) has a perovskite crystal structure and exhibits piezoelectric properties and spontaneous polarization at room temperature. The structures of these two materials have a small lattice mismatch (1.324 % when the unit cell of Fe is rotated by 45 degrees around z-axis). That makes, among other things, it possible to grow epitaxially the Fe film on a $BaTiO_3$ substrate, which was realized in Refs. [28–30], and which makes the Fe/BTO system suitable for *ab initio* studies.

Given the growing interest in controlling ferromagnetic properties via electric and mechanical means, we studied the impact of ferroelectric polarization switching and mechanical striction on the magnetization of Fe layers. The specific aim of this research is to investigate the feasibility of actively controlling the spin dynamics and magnetic anisotropy in ferroelectric/ferromagnetic heterostructures through external electric field and lattice strain modulation. This approach leverages magnetoelectric coupling to enable reversible and energy-efficient manipulation of magnetic and electronic properties within the magnetic layer by tuning the ferroelectric polarization or domain structure via applied electric fields. Such electric-field control of spin dynamics holds significant promise for the development of reconfigurable and low-power magnonic and spintronic devices.

2. Method and calculation parameters

All calculations were carried out based on the density functional theory (DFT) [31]. Exchange and correlation effects were taken into account using the generalized gradient approximation (GGA) with PBE (Purdue, Burke, and Ernzerhoff parameterization) functionals [32]. The

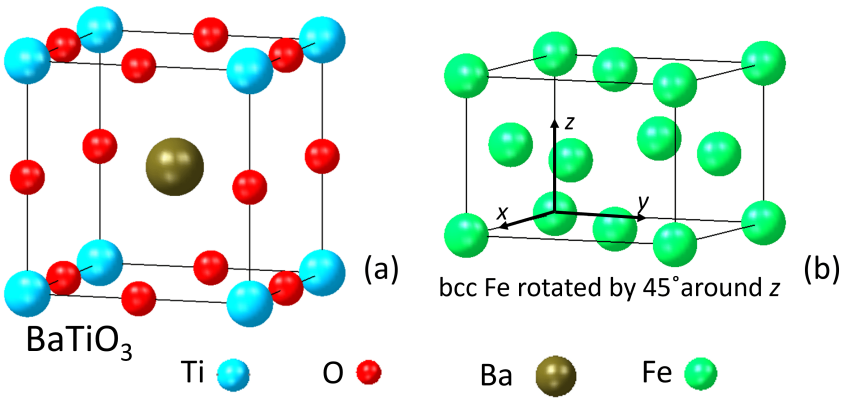

Figure 1. (a) Bulk structure of $BaTiO_3$, (b) bcc Fe rotated by 45 degrees around z-axis. Titanium (Ti), oxygen (O), barium (Ba), and iron (Fe) atoms are represented in blue, red, brown, and green, respectively.

Kohn-Sham equations were solved using projectively extended wave potentials and wave functions [33]. All calculations were performed using the VASP (Vienna ab initio Simulation Package) program [34], integrated into the MedeA program [35]. The plane wave cutoff was set at 400 eV, the criterion for the convergence of atomic relaxation was 0.02 eV/Å, and the condition for the convergence of self-consistent calculations was the invariance of the total energy of the system with an accuracy of 10^{-5} eV. Brillouin zones were sampled using Monkhorst-Pack grids [36], including $7 \times 7 \times 7$ k-points for bulk $BaTiO_3$ and bcc Fe structures, and the density of electronic states was calculated using the linear tetrahedron method [37]. For $Fe/BaTiO_3$ and Fe film heterostructures, k-points of $7 \times 7 \times 1$ with Gaussian smearing of 0.05 eV were used. To account for strong correlations between d-shell electrons, calculations were performed within the GGA+U method using a simplified approach proposed by Dudarev et al., with applied additional local correlations U_{eff} equal to 4.4 eV and 4.6 eV for the $3d$ orbitals of Ti and Fe, respectively [38].

Fig. 1 shows the unit cell of $BaTiO_3$ (Fig. 1a), rotated by 45 degrees around z-axis bcc Fe (Fig. 1b), used to construct the heterostructure.

This rotation was performed in order to contract the heterostructure with matching lattice parameters. We will explain that in more detail in the following section, where bulk properties will be analysed. The $Fe/BaTiO_3$ heterointerface was constructed so that 7 atomic layers of iron were neighboring 11 layers of BTO without a vacuum region, forming a periodic structure (we will refer further to Fe/BTO@7/11 notation). In Ref. [19], the Fe thickness dependence was evaluated, showing a consistency of results above 4 Fe atomic layers (Fig. 2a). The iron atoms are positioned at the interface so that they are directly above the oxygen atoms of the TiO_2 layer. This type of interface construction has the lowest energy of all possible configurations [15]. All coordinates of atoms in the middle three atomic layers of $BaTiO_3$ were fixed during the optimization process to simulate substrate conditions as in real experimentally grown heterostructures [28–30]. Fixing central layers helps to simulate the bulk-like behavior of the substrate, maintaining its structural integrity while allowing the interface and overlayer layers to relax and adapt to interactions. This approach reduces computational cost and avoids unrealistic distortions of the substrate.

The determination of magnetic anisotropy energy (MAE) involves the calculation of the energy difference for the system with magnetization aligned along various crystallographic axes. For heterostructure, we examined the in-plane direction [110], as well as the out-of-plane component

[001]. The MAE for the heterostructure was calculated as a difference in the system's energies when spins are oriented along [*uvw*] and the most favorable direction (easy axis):

$$\mathrm{MAE} = E_{[uvw]} - E_{\mathrm{easy}}. \tag{1}$$

3. Results

3.1. Properties of bulk components

First, the structural properties of Fe and BTO in the bulk phase were calculated. The obtained lattice parameters and the magnetic moment's value were in good agreement with previous *ab initio* and experimental studies [2, 15, 39]. Relaxation was carried out with the possibility of expanding the volume of the crystal lattice. The obtained values of lattice parameters were used to simulate the Fe/$BaTiO_3$ heterostructure. For BTO, $a = b = 4.00$ Å, $c = 4.02$ Å (experimental values are $a = b = 4.00$ Å, $c = 4.02$ Å) [39]. For Fe, $a = b = c = 2.87$ Å before rotation along the z-axis, and after, $a = b = 4.05$ Å, with the magnetic moment of 2.99 μ_B (experimental values are $a = b = c = 2.87$ Å, the magnetic moment of 2.20 μ_B). The Fe lattice parameter was equated to the BTO lattice parameter to construct the heterostructure, so the mismatch between the crystal lattice parameters was 1.32 %.

3.2. Properties of Fe/BTO@7/11 heterostructure

The Fe/$BaTiO_3$ heterostructure was contracted at the next stage by the procedure described in Sec. 2. The unit cell used is shown in Fig. 2a, with displacements obtained after optimization within the parameters used for the bulk phases of BTO and Fe. Note that in contrast to previ-

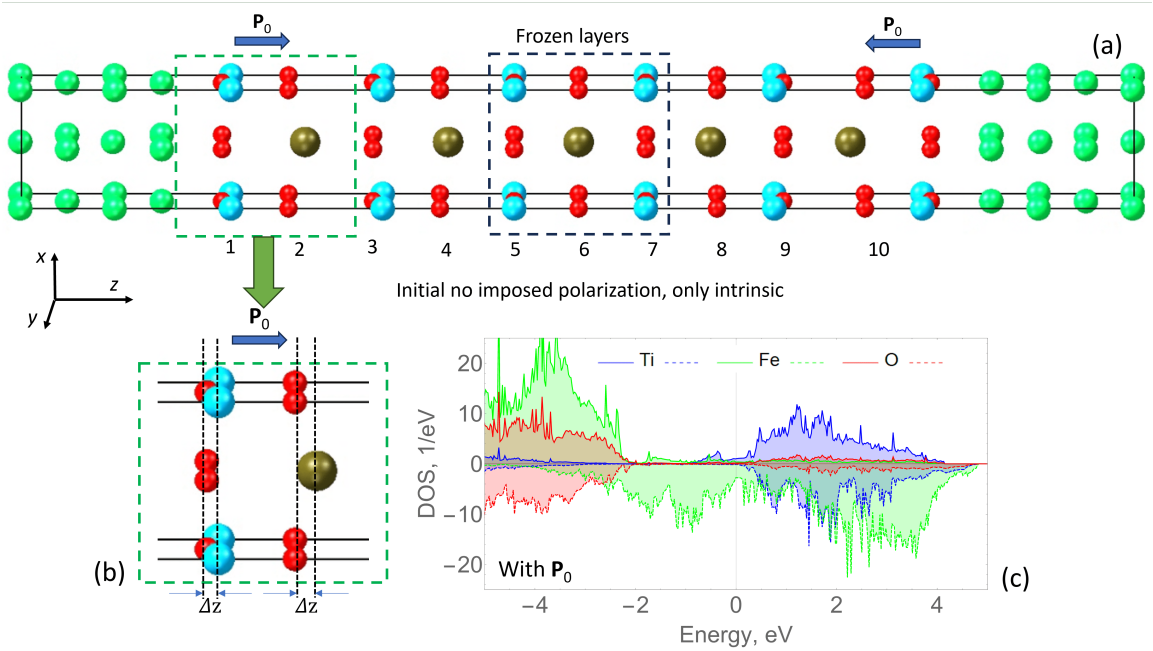

Figure 2. (a) Optimized Fe/BTO@7/11 heterostructure with (b) specified displacement of atoms and (c) corresponding atom-resolved density of states. The numbers $1 - 11$ show the atomic layers in the BTO slab, with interfacial layers being 1 and 11. The black arrow indicates the ferroelectric polarization, denoted as $\mathbf{P}_0$, and directed toward the BTO slab on both sides. Titanium (Ti), oxygen (O), barium (Ba), and iron (Fe) atoms are represented in blue, red, brown, and green, respectively.

ously published theoretical works for Me/BTO (Me = Fe, Co, Ni) interfaces, in our calculations,

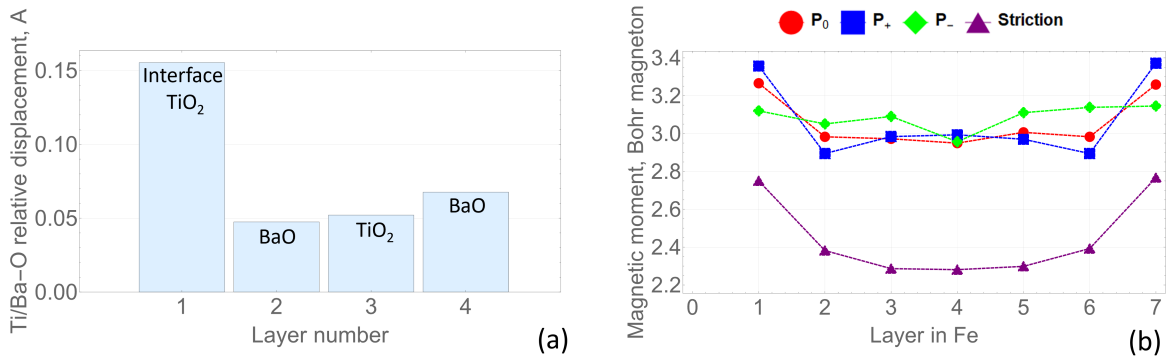

Figure 3. (a) Relative Ti/Ba–O displacements in BTO layers along z direction (as in Fig. 1c) and Fig. 2a and (b) distribution of magnetic moments in the Fe slab in all considered cases.

we simulate the substrate conditions of real experimental realization [28–30]. To do that, the coordinates of the atoms located in layers numbered 5, 6, and 7 were frozen. These layers are marked with a frame on the graph. In the optimized heterostructure, the intrinsic polarization is directed toward the central frozen layers of the ferroelectric slab.

The density of states plot with atom resolution is presented in Fig. 2b. The resulting plot shows the presence of hybridization between Fe and Ti states, as there is an overlap on the energy scale near the Fermi level. In the graph, the $2p$ orbitals of oxygen atoms are located significantly below the Fermi energy and overlap with the $3d$ states of Fe. The maximum DOS of $3d$ states of Ti is located approximately 1.5 eV above the Fermi energy and overlaps well with the $3d$ states of Fe. Moreover, Fe and Ti orbitals are only present near the Fermi level, contributing to the interface conductivity.

Next, the structural analysis, examining Ti-O and Ba-O displacements that appeared after optimization in the ferroelectric layer (shown in Fig. 3), was carried out. As seen from the plot, as a result of the optimization process, relative Ti/ Ba-O displacements are found to vary, which imposes a significant ferroelectric polarization due to the sequence of positively and negatively charged atomic sub-layers. Note that the 5, 6, and 7 layers have no displacement since they were frozen. The biggest displacement was found for the interfacial TiO_2 layers of 0.15 Å. The other displacements are of the same order of approximately 0.05 Å. With respect to the middle layers, the distribution is symmetrical with slight variations. The magnitudes of displacements were of the same order as in previous publications for Fe/BTO and Ni/BTO interfaces [5, 17].

Similarly, a distribution of magnetic moments of Fe atoms in the ferromagnetic layer was obtained (Fig. 3b). The mean magnetic moment of Fe ions varies from 2.94 μ_B to a maximum of 3.1 μ_B, which is 0.11 μ_B more than that of bulk Fe (2.99 μ_B). Maximal values correspond to the 1 and 7 layers, while for all other layers, the magnetic moment is approximately the same, with a mean value of 2.98 μ_B.

3.3. Effect of changing the direction of BTO polarization on the magnetic properties of Fe

To test the effect of changing the direction of ferroelectric polarization on the magnetic properties of the ferromagnet, the displacement values of the Ti and Ba atoms from the oxygen atoms were increased first by approximately 0.2 Å, which was denoted as $\mathbf{P}_+$ polarization (increased toward BTO). Fig. 4 presents the resulting unit cell structure and DOSes. It can be seen, atomic states near the Fermi level changed significantly as a result of varying the direction of ferroelectric

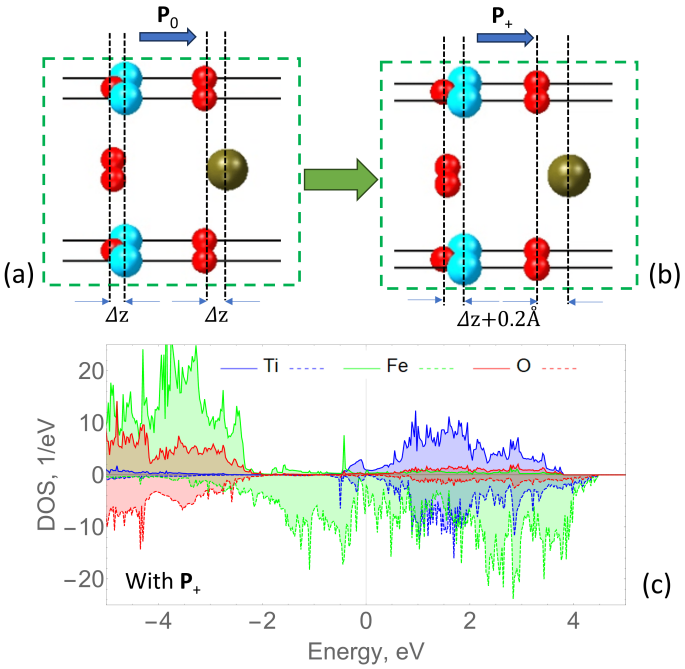

Figure 4. (a) Fe/BTO@7/11 heterostructure with initial ($\mathbf{P}_0$) polarization directed towards ferroelectric slab as in the optimized heterostructure, (b) same heterostructure with increased initial polarization directed towards the ferroelectric ($\mathbf{P}_+$). (c) Partial DOS for Fe, Ti, and O atoms located at the interface. Titanium (Ti), oxygen (O), barium (Ba), and iron (Fe) atoms are represented in blue, red, brown, and green, respectively.

polarization. Partial DOSes, presented in Fig. 4b, show increased contribution of Fe states near the Fermi level and reduced density of Ti states. Besides, a slight increase in total DOS at the Fermi level is observed, indicating an increase in conductivity with additional polarization.

A distribution of magnetic moments of Fe atoms in the ferromagnetic layer at $\mathbf{P}_+$ polarization is plotted in Fig. 3b. In this case, there is a slight increase in the maximal Fe magnetic moment near the interface, which reaches $3.37\,\mu_B$ and has a $0.38\,\mu_B$ difference from that of bulk Fe ($2.99\,\mu_B$). As in the previous $\mathbf{P}_0$ polarization case, maximal magnetic moment is observed for the 1 and 7 layers next to the interface. All other layers have approximately the same magnetic moment, very close to the initial values.

At the next stage, the oxygen ions were shifted in the opposite direction to the initial optimized positions with respect to the Ti and Ba atomic planes. That case corresponds to polarization with opposite (denoted as $\mathbf{P}_-$) direction towards the ferromagnetic slab of Fe. The resulting cell is presented in Fig. 5a. At this polarization, we can observe no significant contribution of Ti states near the Fermi level, as seen from Fig. 5b. Instead, the Fermi level shifted down in the energy scale so that now oxygen states are close to the Fermi level with almost symmetrical spin-up and spin-down components. And since oxygen states cross the Fermi-level, these states take part in the interface conductivity, whereas Ti states appear only above 1 eV.

A distribution of magnetic moments of Fe atoms in the ferromagnetic layer at $\mathbf{P}_-$ polarization is presented in Fig. 3b. The Fe magnetic moment varies in the range $2.96-3.15\,\mu_B$, thus there is a slight decrease of the maximal Fe magnetic moment with respect to the $\mathbf{P}_0$ case, and maximum corresponds to the interfacial layers, and the difference with the bulk Fe ($2.99\,\mu_B$) is $0.16\,\mu_B$. Inner Fe layers have constant magnetic moments, which are approximately the same.

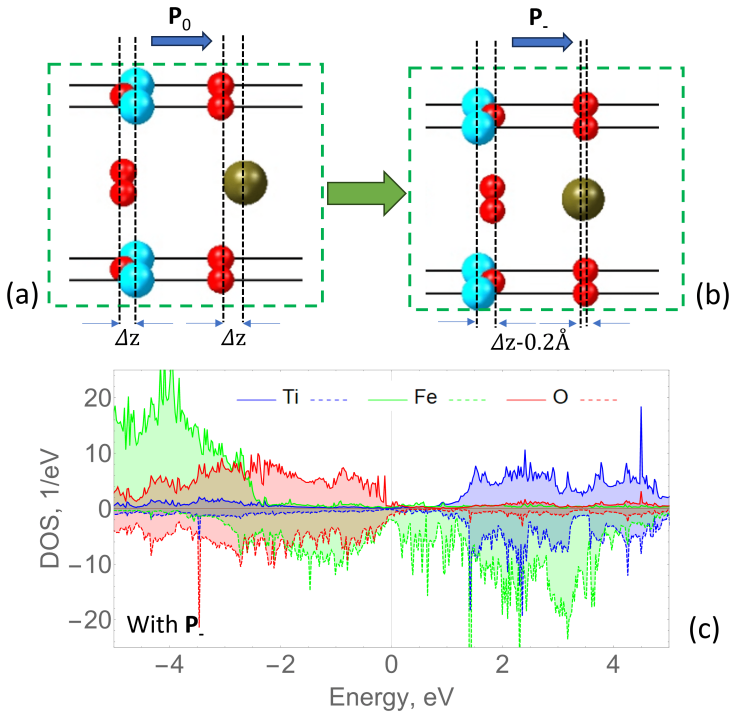

Figure 5. (a) Fe/BTO@7/11 heterostructure with opposite ($\mathbf{P}_-$) to the optimized ($\mathbf{P}_0$) polarization directed towards ferroelectric slab as in the optimized heterostructure, (b) partial DOS for Fe, Ti, and O atoms located at the interface. Titanium (Ti), oxygen (O), barium (Ba), and iron (Fe) atoms are represented in blue, red, brown, and green, respectively.

To sum up, Table 1 contains the DOS contribution at the Fermi level for varied polarizations. This data is presented to comparatively analyze the conductivity via the change of DOS at the Fermi level, so that a higher DOS at the Fermi level means more carriers and higher conductivity. It is seen that the increase of polarization leads to the increase of conductivity, whereas the change of polarization decreases DOS contribution at the Fermi level and conductivity accordingly.

Table 1. The MAE ($E_{110} - E_{001}$) calculated per Fe ion in the Fe/BTO@7/11 heterostructure with considered polarization types.

	DOS at Fermi level, 1/eV	MAE/Fe, meV
$\mathbf{P}_0$	4.364	6.58
$\mathbf{P}_+$	4.888	41.89
$\mathbf{P}_-$	3.976	−3.74

3.4. Magnetic anisotropy characteristics calculations with varied polarization

To analyze the impact of ferroelectric polarization on the magnetic properties of the Fe/BTO@7/11 heterostructure, we calculated the MAE as the energy difference between the magnetization orientations along the [110] and [001] crystallographic directions, defined as ($E_{110} - E_{001}$) and calculated per Fe ion. The calculated data is collected in Table 1. The choice of these particular axes is motivated by the intrinsic structural and electronic properties of the system. The [001] direction corresponds to the out-of-plane axis, aligned with the natural polarization axis of BTO, whereas the [110] direction lies within the interfacial plane, where magnetoelectric and magne-

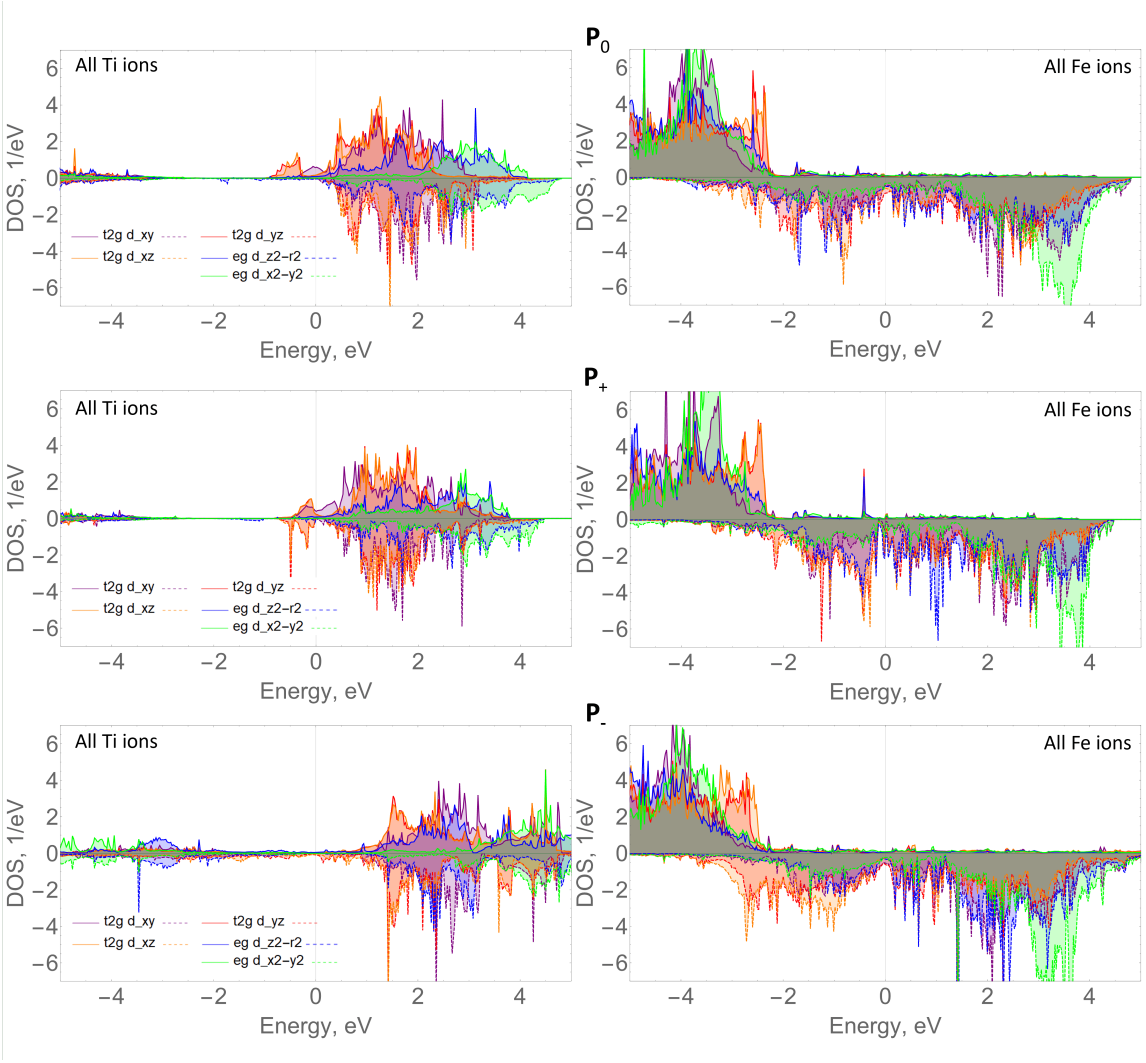

Figure 6. Orbital-resolved density of states Fe/BTO@7/11 heterostructure with initial ($\mathbf{P}_0$), additional ($\mathbf{P}_+$) and opposite ($\mathbf{P}_-$) polarization directions.

tostriction effects are strongly pronounced due to strain and charge redistribution. By comparing these two directions, we can quantify the competition between in-plane and out-of-plane magnetic anisotropies, which is crucial for understanding how electric polarization influences the magnetic easy axis.

As seen from the MAE/Fe column of Table 1, the heterostructure with initial $\mathbf{P}_0$ polarization possesses out-of-plane anisotropy with respect to the interface plane. The increase of polarization in the same direction leads to a significant rise in MAE with the same sign. However, the change of the polarization to the opposite direction towards the ferromagnetic slab of Fe leads to the reorientation of the magnetization axis to the in-plane direction. The obtained results agree well with findings from Ref. [19].

The nature of magnetic properties can be understood from the partial density of states (DOS) plots. Fig. 6 shows the spin-polarized, orbital-resolved density of states for the $3d$ orbitals of Ti and Fe of the Fe/BTO@7/11 heterostructure with three considered polarization types. In the initial optimized Fe/BTO@7/11 heterostructure (Fig. 6 $\mathbf{P}_0$), the main contribution to the electronic states at the Fermi level, which was set to zero in the graphs, comes from the spin-up component of d_{xy} orbital of Ti and spin-down component of d_{yz} and d_{xz} levels of Fe.

As a result of increased polarization, Fig. 6 $\mathbf{P}_+$, the change of orbital filling is not crucial in comparison with the previous $\mathbf{P}_0$ case. Ti states have a similar case to the previous $\mathbf{P}_0$ case; just d_{xz} and d_{yz} are more pronounced at the Fermi level. Contrarily, Fe states near the Fermi level changed significantly so that now we see the most contributions from d_{xz}, d_{yz}, and $d_{z^2-r^2}$ of the spin-down component. Overall, such an inhomogeneous filling of states does not change dramatically the easy out-of-plane axis; however, the difference between energies of in-plane and out-of-plane directions is increased with respect to the $\mathbf{P}_0$ case (Table 1).

Further, the polarization direction has been changed to the opposite of the initial ($\mathbf{P}_0$) direction. This $\mathbf{P}_-$ polarization leads to the significant reconstruction of the electronic state. As seen in Fig. 6, for $\mathbf{P}_-$ polarization, DOS for Ti ions does not have any pronounced anisotropy of spin filling, and overall electronic states near the Fermi level are close to zero. As for Fe atoms, the most contribution is from spin-down d_{yz} and slightly less from d_{xy} orbitals, and almost twice less from other orbitals. This substantial variation of the local DOSes might be a reason for a change of the easy magnetization axis from out-of-plane to the in-plane direction. As seen from Table 1, the strength of MAE is the same order as for the $\mathbf{P}_0$ case but with the opposite sign. Consequently, the change of polarization is capable of influencing the strength and direction of magnetic anisotropy in the Fe/BTO@7/11 heterostructure.

As we have seen from the total plots for the separate ions, the oxygen levels shift up in the energy scale for $\mathbf{P}_-$ polarization, and that is why the orbital-resolved DOS plots were constructed as well and presented in Fig. 7. It follows from the partial DOS analysis of $2p$ orbitals of oxygen that most of these states are degenerated and produce minor magnetization. These states are located predominantly in the valence band of the Fe/BTO@7/11 heterostructure with initial $\mathbf{P}_0$ and imposed polarization $\mathbf{P}_+$ and have a negligible contribution near the Fermi level. The situation changes drastically as soon as the polarization is directed toward the ferromagnetic layer. In that situation, the oxygen ions are shifted towards the BTO slab as depicted in Fig. 5 and hybridized with Fe states.

3.5. Reverse magnetostriction effect

To test the effect of striction along the x and y-axes on the magnetic properties of the ferromagnetic material, the entire Fe/BTO@7/11 heterostructure was simultaneously compressed along the y-axis by 0.2 Å and expanded along the x-axis (and oppositely) by the same amount. In Fig. 3b, the distribution of magnetic moments along Fe layers for the heterostructure under anisotropic striction is shown with a pronounced decrease in the magnetic moments. The values varied in the $2.28 - 2.77\,\mu_B$ range, thus, there is a $0.22\,\mu_B$ difference between the maximal value with the magnetic moment of the bulk Fe ($2.99\,\mu_B$). As in the previously considered cases with varied polarization, maximal magnetic moment is observed for the 1 and 7 layers, while all other layers have the mean magnetic moment of $2.33\,\mu_B$. Besides, in that case, a big difference between the magnetic moments of the interface layer and others was obtained.

Further, the easy magnetization axis change was evaluated when the axial stress was applied to the in-plane x-direction. The MAE was calculated as $E_{[100]}$-$E_{[010]}$ and equals 3.67 meV/Fe. The easy and hard magnetization axes were found to be [010] and [100], respectively. It means that applied uniaxial stress in one direction makes that direction the hard axis and the perpendicular direction – the easy one.

Similarly to the previous section, the change of easy magnetization direction was analyzed via DOS calculations with orbital resolution as presented in Fig. 8.

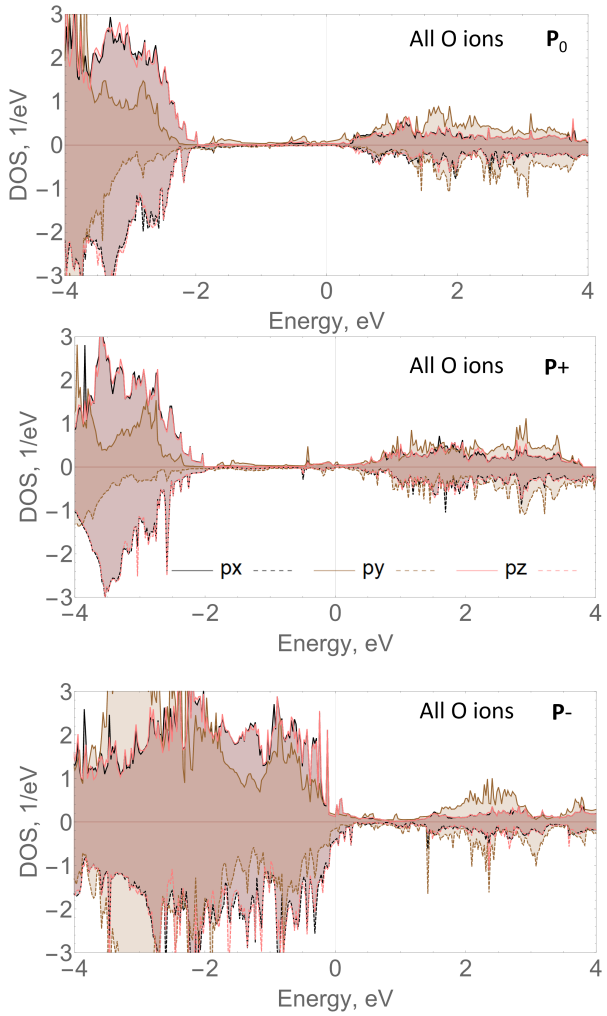

Figure 7. Orbital-resolved DOS for oxygen ions for Fe/BTO@7/11 heterostructure with initial ($\mathbf{P}_0$), additional ($\mathbf{P}_+$) and opposite ($\mathbf{P}_-$) polarization directions.

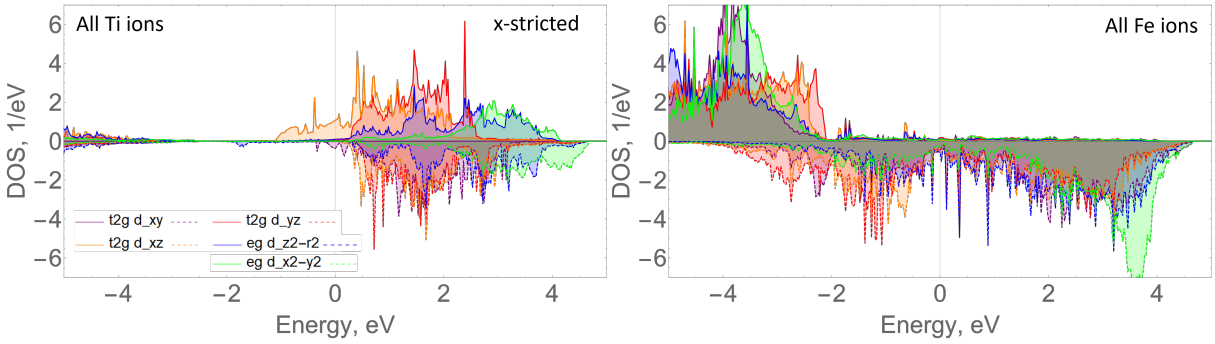

Figure 8. Orbital-resolved DOS for Fe and Ti atoms in the Fe/BTO@7/11 heterostructure with uniaxial striction in x-direction.

For the heterostructure stricted in x-direction, the orbital-resolved DOS shows the most difference between spin-up and down components for d_{xz} and slightly less for d_{xy} orbitals of Ti, as well as Fe d_{xz} and Fe $d_{z^2-r^2}$, which generally makes perpendicular to these directions [010] an easy magnetization axis.

4. Conclusion

The structural, electronic, and magnetic properties of the Fe/$BaTiO_3$ ferromagnet/ferroelectric heterostructure have been investigated using density functional theory with inclusion of spin-orbit coupling. Our results demonstrate that different polarization orientations significantly influence the electronic charge distribution and, consequently, the magnetic ordering within the ferromagnetic layer, supporting the concept of ferroelectric control over conductivity and preferred magnetization direction.

Specifically, we found that the most energetically favorable configuration features polarization pointing away from the interface with the Fe layer and toward the center of the ferroelectric $BaTiO_3$ slab. In this state, the heterostructure exhibits metallic behavior at the interface with predominant contributions from $3d$ states of Fe and Ti. Moreover, the heterostructure exhibits uniaxial magnetic anisotropy, with the easy axis of magnetization oriented perpendicularly to the interface plane. This uniaxial behavior can be modulated by the direction of ferroelectric polarization, which induces a substantial redistribution of the spin-polarized states.

When additional polarization is imposed in the same direction, it enhances both the interfacial conductivity and the magnitude of the magnetic anisotropy energy (MAE) while preserving the out-of-plane orientation of the easy axis. In contrast, reversing the polarization direction induces a significant redistribution of the electronic states, resulting in a reorientation of the magnetization easy axis into the plane of the interface.

Finally, the effect of in-plane uniaxial compressive strain applied parallel to the interface was examined as an additional mechanism of spin-state manipulation. It was found that compression along the x-direction favors the [010] direction as the easy axis of magnetization, while [100] – as the hard axis. These results highlight the sensitivity of magnetic anisotropy to spin-lattice interactions and magnetoelastic coupling, offering an additional route for strain-mediated control of magnetization orientation in the ferromagnet/ferroelectric heterostructure.

In summary, two spin-related effects were demonstrated in the Fe/$BaTiO_3$ heterostructure. First, the magnetoelectric coupling enables direct control of spin dynamics using electric fields, allowing for low-power manipulation of magnetic states and excitations. The second, reverse magnetostriction provides a direct mechanical route to influence spin dynamics, making it a crucial effect in modern magnetics and spintronics research. Thus, these results open new avenues for the creation of devices using control of magnetic states of the films by electric field.

Acknowledgments

The work of I.Piyanzina (Gumarova) was supported by the grant 24PostDoc/2-2F006. The work of R. Mamin, A. Kamashev and I. Piyanzina was supported by the government assignment for the FRC Kazan Scientific Center of RAS. Computational resources were provided by the Armenian National Supercomputing Center (ANSCC).

References

1. Revathy R., Kalarikkal N., Varma M. R., Surendran K. P., *J. All. Compd.* **889**, 161667 (2021).

2. Zhao Y., Peng R., Guo Y., Liu Z., Dong Y., Zhao Sh., Li Y., Dong G., Hu Y., Zhang J., Peng Y., Yang T., Tian B., Zhao Y., Zhou Z., Jiang Z., Luo Z, Lui M., *Adv. Funct. Mater.* **31**, 2009376 (2021).

3. Borek S., Braun J., Minár J., Kutnyakhov D., Elmers H-J., Schönhense G., Ebert H., *J. Phys.: Condens. Matter.* **28**, 436004 (2016).
4. Gao H., Lin T., Yan Y., Fu K., Liu Y., Liu X., *J. Phys. Chem. Chem. Phys.* **22**, 18284 (2020).
5. Venkataiah G., Gorige V., Swain A., Komatsu K., Itoh M., Taniyama T., *Rapid Res. Lett.* **11**, 1700294 (2017).
6. Fechner M., Maznichenko I. V., Ostanin S., Ernst A., Henk J., Bruno P., Mertig I., *Phys. Rev. B* **78**, 212406 (2008).
7. Li P., Chen A., Li D., Zhao Y., Zhang S., Yang L., Liu Y., Zhu M., Zhang H., Han X., *Adv. Mater.* **26**, 4320 (2014).
8. Ortega N., Kumar A., Scott J. F., Katiyar R. S., *J. Phys.: Condens. Matter.* **27**, 504002 (2015).
9. Spaldin N., Ramesh R., *Nature Mater.* **18**, 203 (2019).
10. Kumari S., Pradhan D. K., Katiyar R. S., Kumar A., *Metal Oxides.* **29**, 571 (2019).
11. Vaz C., Staub U., *J. Phys.: Condens. Matter.* **27**, 500301 (2015).
12. Leksin P. V., Garif'yanov N. N., Garifullin I. A., Schumann J., Vinzelberg H., Kataev V., Klingeler R., Schmidt O.G., Büchner B., *Appl. Phys. Lett.* **97**, 102505 (2010).
13. Kamashev A. A., Garif'yanov N. N., Validov A. A., Schumann J., Kataev V., Büchner B., Fominov Y. V., Garifullin I. A., *Phys. Rev. B* **100**, 134511 (2019).
14. Kamashev A. A., Garif'yanov N. N., Validov A. A., Kataev V., Osin A. S., Fominov Y. V., Garifullin I. A., *Phys. Rev. B* **109**, 144517 (2024).
15. Duan C. G., Jaswal S. S., Tsymbal E. Y., *Phys. Rev. Lett.* **97**, 047201 (2006).
16. Valencia S., Crassous A., Bocher L., Garcia V., Moya X., Cherifi R. O., Deranlot C., Bouzehouane K., Fusil S., Zobelli A., Gloter A., *Nature Mater.* **10**, 753 (2011).
17. Li W., Lee J., Demkov A. A., *J. Appl. Phys.* **131**, 054101 (2022).
18. Qu Z., Huang C., Wu S., Wu F., Wang J., Deng K., Kan E., *Phys. Rev. B* **110**, L161408 (2024).
19. Ochirkhuyag T., Kioussis N., Rhim S. H., Odkhuu D., **127**, 24467 (2023).
20. Zhang Y., Wang Z., Wang Y., Luo C., Li J., Viehland D., *J. Appl. Phys.* **115**, 084101 (2014).
21. Zhang Y., Li J., Dai B., Ni J., Ren Y., Tan S., *Ceram. Int.* **45**, 7262 (2019).
22. Zhou Z., Howe B. M., Liu M., Nan T., Chen X., Mahalingam K., Sun N. X., Brown G. J., *Sci. Rep.* **5**, 7740 (2015).
23. Okabayashi J., Miura Y., Taniyama T., *Quantum Mater.* **4**, 21 (2019).
24. Zemp Y., Trassin M., Gradauskaite E., Gao B., Cheong S. W., Lottermoser T., Fiebig M., Weber M. C., *Phys. Rev. B* **109**, 184417 (2024).
25. Xu S., Wang J., Chen P., Jin K., Ma C., Wu S., Guo E., Ge C., Wang C., Xu X., Yao H., *Nat. Commun.* **14**, 2274 (2023).
26. Bagri A., Jana A., Panchal G., Chowdhury S., Raj R., Kumar M., Gupta M., Reddy V. R., Phase D. M., Choudhary R. J., *ACS Appl. Mater. Interfaces* **15**, 18391 (2023).

27. Sahoo S., Mahapatra P. K., Choudhary R. N. P., Nandagoswami M. L., Kumar A., *Mater. Res. Express* **3**, 065017 (2016).

28. Panchal G., Kojda D., Sahoo S., Bagri A., Singh Kunwar H., Bocklage L., Panchwanee A., Sathe V. G, Fritsch K., Habicht K., Choudhary R.J., *Phys. Rev. B.* **105**, 224419 (2022).

29. Fang Z., Peng Y., Li H., Liu X., Zhai J., *Crystals* **15**, 337 (2025).

30. Radaelli G., Petti D., Plekhanov E., Fina I., Torelli P., Salles B. R., Cantoni M., Rinaldi C., Gutiérrez D., Panaccione G., Varela M., *Nat. Commun.* **3**, 3404 (2014).

31. Kresse G., Furthmüller J., *Comput. Mater. Sci.* **6**, 15 (1996).

32. Perdew J. P., Burke K., Ernzerhof M., *Phys. Rev. Lett.* **77**, 3865 (1996).

33. Blöchl P. E., *Phys. Rev. B* **50**, 17953 (1994).

34. Kresse G., Furthmüller J., *Phys. Rev. B* **54**, 11169 (1996).

35. MedeA version 3.10; MedeA is a registered trademark of Materials Design, Inc., San Diego, USA.

36. Monkhorst H. J., Pack J. D., *Phys. Rev. B* **13**, 5188 (1976).

37. Blöchl P. E., Jepsen O., Andersen O. K., *Phys. Rev. B* **49**, 16223 (1994).

38. Dudarev S. L., Botton G. A., Savrasov S. Y., Humphreys C. J., Sutton A. P., *Phys. Rev. B* **57**, 1505 (1998).

39. Zali N. M., Mahmood C. S., Mohamad S. M., Foo C. T., Murshidi J. A., *AIP Conf. Proc.* **1584**, 160 (2014).